Advances in the expression and purification of human PARP1: a user-friendly protocol

Carlota J. F. Conceição[a,b], Bruno Salgueiro[c], Paulo A. Ribeiro[b], Maria Raposo[b], Elin Moe[c, d, *]

[a] CEFITEC, Department of Physics, NOVA School of Science and Technology, Universidade NOVA de Lisboa, 2829-516 Caparica, Portugal; cj.conceicao@campus.fct.unl.pt

[b] Laboratory of Instrumentation, Biomedical Engineering and Radiation Physics (LIBPhys-UNL), Department of Physics, NOVA School of Science and Technology, Universidade NOVA de Lisboa, 2829-516 Caparica, Portugal; pfr@fct.unl.pt; mfr@fct.unl.pt

[c] Institute of Chemical and Biological Technology (ITQB NOVA), The New University of Lisbon, Oeiras, Portugal; brunosalgueiro@itqb.unl.pt; elinmoe@itqb.unl.pt

[d] Department of Chemistry, UiT – the Arctic University of Norway, Tromsø, Norway.

* Corresponding author: Institute of Chemical and Biological Technology (ITQB NOVA), The New University of Lisbon, Oeiras, Portugal. *E-mail address*: elinmoe@itqb.unl.pt (E.Moe)

Abstract

The PARP1 (Poly (ADP-ribose) polymerase 1) enzyme is essential for single and double-strand break repair in humans. Alterations affecting PARP1 activity have severe consequences for human health and are associated with pathologies like cancer, and metabolic and neurodegenerative disorders. Here, we have developed a fast and easy procedure for the expression and purification of PARP1. Biologically active protein was purified to an apparent purity > 95 %, with only two purification steps. A thermostability analysis revealed that PARP1 possessed improved stability in 50 mM Tris-HCl pH 8.0 (Tm = 44.2 ± 0.3 ^{o}C), thus this buffer was used throughout the whole purification procedure. The protein was shown to bind to DNA and has no inhibitor molecules bound to the active site. Finally, the yield of the purified PARP1 protein is sufficient for both biochemical, biophysical and structural analysis. The new protocol is more effective and produces similar protein quantities in less time.

Keywords: Human PARP1, recombinant expression, purification, protein stabilization, Nano-DSF, Zincon, MS, auto-modification activity

1. Introduction

Poly (ADP-ribose) polymerase 1 (PARP1) belongs to a large protein family with 17 members. The protein can be found in several cellular compartments and is involved in various cellular processes [1]. PARP1 is categorized as a nuclear PARP along with two other members of the family, PARP2 and PARP3 [2]. These three proteins are associated with poly (ADP-ribosyl) (PAR) post-translational modifications, with PARP1 being the major executer [3]. PARP1 is composed of a single chain of 1014 amino acids and contains 6 major domains. Homology with other family members is only observed in the C-terminal domain, where the catalytic domain (CAT) is present [4]. In structural terms, the protein consists of three zinc finger domains (Zn1, Zn2 and Zn3), a BRCT domain (BRCA-1 C-terminus fold), the WGR (Tryptophan-Glycine-Arginine) domain and the CAT domain (comprises the α-helical subdomain (HD) and the ADP-ribosyltransferase fold (ART)) [5,6]. The multiple-domain structure is pivotal for PARP1's numerous biological functions. The protein is primarily associated with DNA damage repair pathways (e.g. BER, NER, among others), but is also involved in events such as transcription, cell cycle regulation and death [4,5].

The role of PARP1 is to detect, bind, and stabilize DNA breaks. DNA repair is then initiated by the addition of poly (ADP-ribose) (PAR) chains to its own BRCT domain, termed PARylation, leading to the recruitment of effector proteins and the release of PARP1 from the damaged site [2,6]. The PARylation process is tightly regulated and proves to be of high importance, if not essential, since PARP1 is capable to both auto- and hetero modify several targets [7]. Deregulation of PARP1 enzymatic activity is often associated with several pathologies, such as inflammatory processes, metabolic disorders, neurodegenerative diseases, ageing and cancer [8–10].

Despite years of extensive studies of PARP1, there are still a lot of questions that remain to be answered regarding its biochemical and biophysical properties, inhibition and structure. However, it is a challenge to obtain high yields of pure biologically active PARP1 enzyme for studies at a molecular level. In this work, we have developed a fast and efficient method for expression and purification of recombinant PARP1, compared to other published work [5,11–14]. The protocol is easy to reproduce and results in pure, stable, and biologically active recombinant protein in amounts sufficient for characterization, structural and radiation experiments.

2. Materials and Methods

2.1. Gene Cloning, Protein Expression and Purification

2.1.1. *Gene cloning*

The gene encoding for human PARP1 was amplified from the plasmid pCMV-PARP1-3xFlag-WT which was a gift from Thomas Muir (Addgene plasmid # 111575; http://n2t.net/addgene:111575; RRID:Addgene_111575) [15]. The primers used for gene amplification and cloning are shown in Table 1. Nucleotides encoding an N-terminal 6x-Histag sequence and a TEV cleavage site were included in the amplified PARP1 gene via the primer FDRall. 50 μL reactions contained 1x Phusion Buffer HF, 0.2 mM dNTPs, 10 μM forward and reverse primer, 3% dimethyl sulfoxide and 0.5 U Phusion DNA Polymerase (ThermoFisher). PCR reactions included a 98 °C initial denaturation step (5 min); 30 cycles of denaturation (98 °C for 30 seconds), annealing (55 °C for 1 min) and extension (72 °C for 2 min). A final extension was performed at 72 °C for 7 min. PARP1 amplicons were inserted in the pDest14 expression vector following the Gateway Cloning system (ThermoFisher) recommendations. Vectors selected for the cloning processes were entry vector pDONR221 and destination vector pDest14. The correct clones were verified by sequencing using the Eurofins Genomics services.

Table 1

Primer sequences used for the amplification and cloning of the PARP1 gene.

Name	Nucleotide Sequence
FPPARP1	5'-CATCACCATCACCATCACGAAAACCTGTATTTCCAGGGAGCAATGGCGGAGTCTTCGGATAAG-3'
RPPARP1	5'-GGGGACCACTTTGTACAAGAAAGCTGGGTCTCACCACAGGGAGGTCTTAAA-3'
FDRall	5'-GGGGACAAGTTTGTACAAAAAAGCAGGCTTCGAAGGAGATAGAACCATGCATCACCATCACCATCAC- 3'

2.1.2. *Protein Expression – Small to large scale*

Initial small-scale expression tests (10 ml) were performed with seven different *Escherichia coli* expression strains. Rosetta™, Rosetta™ 2, Rosetta-gami ™ 2, Rosetta™ pLysS 2, Tuner (DE3), pLysS star (DE3) and Lemo 21 (DE3) were transformed with pDest14 containing the gene encoding PARP1. Different growth media (LB Broth (LB), Power Broth (PB) and Auto-induction),

growth temperatures (37 °C and 18 °C) and incubation time (2 hours, 3 hours and overnight) were tested. Induction of protein expression was performed by addition of 1 mM isopropyl β-D-1- thiogalactopyranoside (IPTG). Culture media was supplemented with Ampicilin (200 μg/ml) and Chloramphenicol (34 μg/ml). Cells were harvested by centrifugation and lysed using 200 μL lysis buffer (50 mM Tris-HCl pH 7.5, 150 mM NaCl, 5 mM $MgCl_2$, 0.1 mg/ml lysozyme, 1 μg/ml DNase) and subjected to three cycles of freeze and thaw in liquid nitrogen. Centrifugation (15000 xg, 10 min, 4 °C) was performed to recover cytoplasmatic fractions (soluble fraction) and the pellet (insoluble fraction). The pellet was resuspended in 50 μL 1 % SDS and heated (95 °C, 5 min). Fractions were analysed on 10 % and 12.5% Tris-glycine-SDS-PAGE gel, stained with Blue-Safe (NZYTech). Protein expression of PARP1 was confirmed by Western blot (Wet-System BioRad) (protocol depicted in next subsection). The expected molecular mass of PARP1 is 114 kDa. After determination of the best strain for PARP1 expression, a scale-up was performed in 1 L LBmedia.

Recombinant PARP1 expression was performed using an adapted protocol from Langelier et al., [16]. 25 ml of LB broth supplemented with Ampicillin (200 μg/ml), Chloramphenicol (34 μg/ml) and 1 % glucose was inoculated with Rosetta 2 (DE3) *E. coli* colonies, transformed with the pDest14 vector containing the gene encoding full-length PARP1. The culture was grown overnight at 37 °C and 150 rpm. 10 ml of the overnight culture was used to inoculate 1 L LB medium with 200 μg/ml Ampicillin, 34 μg/ml Chloramphenicol and grown to an OD_{600} = 0.65 at 37 °C at 120 rpm. At this point the culture medium was cooled down in a cold chamber for 30 min and supplemented with 0.1 mM $ZnSO_4$ solution (100 mM stock). Expression was induced by addition of 0.2 mM of IPTG and the culture was grown overnight at 18 °C at 120 rpm. Cells were harvested by centrifugation for 30 minutes at 8000 rpm (Avanti™ J-26 XPI High Performance Centrifuge, with Beckman Coulter JA-10 fixed-angle rotor), 4 °C and stored at -20 °C.

2.1.3. *Protein Purification*

Cells were resuspended in 20 ml of lysis buffer (50 mM Tris pH 8.0, 150 mM NaCl, 5 mM $MgCl_2$, 0.1 mg/ml lysozyme, 1 μg/ml DNase and 1 tablet protease inhibitor cocktail III (Merck Millipore)). Resuspended cells were lysed by repeated freeze-thaw cycles using liquid nitrogen. The cell extract was centrifuged at 17000 rpm (Avanti™ J-26 XPI with Beckman Coulter JA-25.50 fixed-angle rotor) for 30 min at 4 ^{o}C. The supernatant was injected into a pre-equilibrated 1 mL Histrap HP™ column (GE Healthcare) in buffer A (50 mM Tris-HCl pH 8.0, 150 mM NaCl, 0.5 mM TCEP, protease inhibitor cocktail III). The purification steps utilized an AKTA Explorer system (GE Healthcare) implementing both isocratic and gradient methods and employing a flow rate of 1 mL/min. A 5 % buffer B step was included to remove low affinity contaminants and a gradient

of 5-100 % buffer B was employed to elute the target protein. Eluted fractions were assessed by 10 and 12.5 % SDS-PAGE and fractions of interest were pooled. Buffer exchange was performed using a Cytiva HiPrep™ 26/10 Desalting column (Fisher Scientific) and Heparin Buffer A (50 mM Tris-HCl pH 8.0, 75 mM NaCl, 0.1 mM TCEP, 1mM EDTA), with a flowrate of 3 ml/min. Desalted fractions were loaded onto a 5 ml HiTrap Heparin HP™ column (GE Healthcare) for removal of bound DNA. The protein was eluted over a 0-100 % buffer B gradient (50 mM Tris-HCl pH 8.0, 1 M NaCl, 0.1 mM TCEP, 1 mM EDTA) and flowrate of 2 mL/min. Protein fractions eluted were analysed by SDS-PAGE, pooled, and concentrated to approximately 1 mg/ml in a Amicon® Ultra-4 (10 kDa MWCO) (Merck), and flash frozen in liquid nitrogen and stored at -80 ^{o}C. Protein concentration determination was performed using the Bradford method.

PARP1 aliquots of 250 μL were injected and analysed in a Superdex 200 10/300GL (GE Healthcare) in an AKTA Explorer system (GE Healthcare). The elution buffer used was 50 mM Tris-HCl pH 8.0 and 150 mM NaCl.

2.2. Zinc^{2+} Ion Quantification – Zincon (2-carboxy-2'-hydroxy-5'-sulfoformazylbenzene) Assay

1.6 mM Zincon monosodium salt (Thermo Scientific) solution was dissolved in 1 ml 1 M NaOH and diluted in Milli-Q water until the designated final concentration. A stock solution of 51.28 mM borate pH 9.0, 8.2 M urea was prepared for assay incubation and a 40-fold concentrated work solution of $ZnSO_4.7H_2O$ (Merck) [17] was used for construction of a standard metal ion curve. The zinc work solution was prepared from a 100 mM stock. Final concentrations of 0 to 40 μM metal ion and 1 μM of recombinant PARP1 were used in the assay. An initial 10 min incubation of the protein in 50 mM borate pH 9.0, 8 M urea at room temperature was carried out to release zinc ions from the protein's metal cores. The Zincon reagent was used at a final concentration of 40 μM, and the chelation reaction was left to incubate at room temperature for 5 min. Absorbance at 628 nm was recorded in the Spark® multimode microplate reader (Tecan), with a Nunc™ 96-well polystyrene plate (Thermo Scientific). At least three replicas were done and mean values with standard deviation values are presented.

2.3. PARP1 Auto-modification Activity Assay

PARP1 auto-modification activity reactions were conducted following the protocol described by Langelier [16]. Activity reactions were all prepared on ice and incubated at room temperature for 10 min. Reaction solutions used 1 μM protein, 1 μM blunt non-labelled DNA template (Seq.Fw: 5'-AGTACGGTCATCGCG-3' and Seq.Rv: 5'-CGCGATGACCGTACT-3'), 5 mM beta -nicotinamide adenine dinucleotide (β-NAD+) and incubation buffer (20 mM Tris-HCl pH 7.5, 50 mM NaCl, 5 mM $MgCl_2$). Auto-modification reactions were stopped by adding SDS-loading buffer

(15.6 mM Tris, 100 mM EDTA, 2.5% glycerol, 0.2 M β-mercaptoethanol, 0.26% SDS, 0.001% bromophenol blue). Reactions were analysed in 10 % SDS-PAGE gel, stained with BlueSafe (NZYTech) and images were acquired using the Gel Doc EZ System (BIORAD).

2.4. Wet-system Western-Blot

Protein samples were loaded onto 10 SDS-PAGE gels (1.0 mm, 15-well gel) and run at 180 V. Gels were wet transferred in 0.45 μm nitrocellulose filter paper sandwiches 7 x 8.5 cm (BioRAD) previously prepared in 1x Transfer Buffer (25 mM Tris-base 192 mM glycine 0.05 % SDS 20 % methanol). Membranes were blocked for 1h at room temperature in 5 % powdered dry milk solution (1x TBST). Primary (Mouse monoclonal Anti-6x Histag antibody, Catalog No: SAB1305538) and secondary (Goat Anti-Mouse IgG antibody, alkaline phosphatase-conjugated, Catalog No: AP124A) antibodies (Sigma-Aldrich) were diluted (1:6000) in 5 % milk solution and incubated for 1 h at room temperature with gentle shaking. Washes were performed after each antibody incubation with 1x TBST with gentle shaking. Detection was performed with membrane incubation in BCIP®/NBT Liquid Substrate System (Sigma-Aldrich).

2.5. Protein Mass Spectrometry Analysis

Peptide mapping was performed by the UniMS (ITQB/iBET, Oeiras, Portugal) using a nanoLC-MS and Sciex TripleTOF 6600 mass spectrometer. Mass spectra data was processed with Protein Pilot Software v. 5.0 (Sciex) for protein identification, and search was done against the SwissProt protein sequences for *E. coli* and human PARP1 sequence (P09874 – PARP1_HUMAN). A confidence cut-off at least of 95% and percentage of amino acids in protein sequence identified with set cut-off were used for data analysis and peptide identification.

2.6. Nano Differential Scanning Fluorimetry (Nano-DSF)

Real-time monitoring of Intrinsic Tryptophan Fluorescence (ITF) at 330 nm and 350 nm was performed in a Prometheus NT.48 (NanoTemper Technologies) with an excitation wavelength of 280 nm. High-sensitivity capillaries were filled with 10 μl PARP1 at a final concentration of 0.2 mg/ml. A buffer screen comprising 50mM Tris-HCl, 50 mM Tricine, 20 mM HEPES and 50 mM Gly-Gly at pH ranging from 7.0 to 8.0 were assessed. A temperature ramp from 20 to 90 °C at a rate of 1 °C/min, was employed. Emission intensity ratio (Em_{350nm}/Em_{330nm}), was plotted as a function of temperature and first derivatives were calculated using the manufacturer's software (PR.ThermControl, version 2.1.2). Three independent measurements were carried out and mean values are presented.

3. Results and Discussion

3.1. Protein expression tests

Upon achieving positive clones, small scale test expression experiments of PARP1 were carried out. Several *E. coli* strains, growth medium (Luria Broth (LB), Power Broth (PB) and auto-induction) and culture conditions (37 °C 2h-3h and 18 °C overnight) were selected and tested. The *E. coli* strains listed in **Table 2** were selected based on their unique features and suitability for expression of recombinant human proteins.

Table 2. Cell lines tested for expression of PARP1, with X indicating no expression, v indicating expression and – indicating strain not tested).

Strains	**Medium**	**PARP1**	
		18 °C	**37 °C**
Rosetta™	LB	-	X
	PB	-	X
	Auto induction	-	-
Rosetta™ 2	LB	✓ *	X
	PB	-	X
	Auto induction	X	-
Rosetta-gami™ 2	LB	-	X
	PB	-	X
	Auto induction	-	-
Rosetta™ pLysS 2	LB	-	X
	PB	-	X
	Auto induction	-	-
Tuner (DE3)	LB	-	X
	PB	-	X
	Auto induction	X	-
pLysS * (DE3)	LB	-	X
	PB	-	X
	Auto induction	X	-

Lemo 21	LB	-	X
	PB	-	X
	Auto induction	-	-

*in specific growth conditions (see subsection 2.1.2, second paragraph)

The expression tests of PARP1 encompassed a total of 21 conditions (**Fig. 1** and **Supplementary Fig. 1-4**). Among those, Rosetta in LB and PB media presented substantial growth problems, not even achieving the desired OD_{600} for expression induction. Also, an attempt to verify if PARP1 could be expressed in a short time interval (2h) in Rosetta 2 with LB medium at 37 ^{o}C proved to be ineffective (**Supplementary Fig. 4**). Protein expression was induced by the addition of 1 mM IPTG at an optical density (OD_{600}) of 0.65 in all conditions, except for the auto-induction medium.

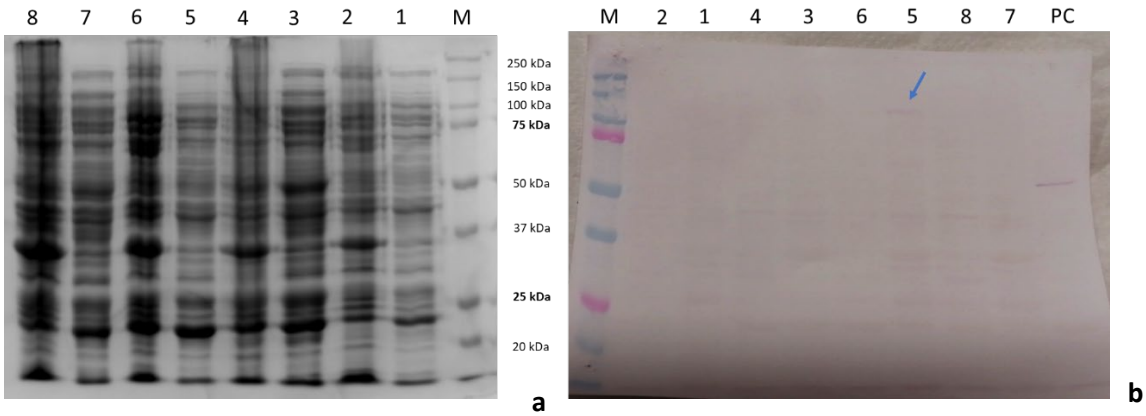

Figure 1. PARP1 (114 kDa) expression tests in different cell lines and media conditions. a) SDS-PAGE gel (10%) of soluble and insoluble fractions of PARP1 protein; b) Western blot results with identification of PARP1 expression in well 5. M – Precision Plus Protein™ Dual colour standard (BioRad); 1- Tuner Auto-induction medium (soluble fraction); 2 - Tuner Auto-induction medium (insoluble fraction); 3 – pLysS* Auto-induction medium (soluble fraction); 4 – pLysS* Auto-induction medium (insoluble fraction); 5 – Rosetta 2 LB (soluble fraction) (adapted Langelier protocol); 6 - Rosetta 2 LB (insoluble fraction) (adapted Langelier protocol); 7 – pLysS* LB (soluble fraction); 8 – pLysS* LB (insoluble fraction); PC- positive control (PARP1 WGR-CAT construct).

Due to the difficulty of obtaining PARP1 expression, a modified protocol from Langlier et al. [16] was tested following the methodology described in subsection 2.1.2. This protocol incudes the use of a pre-inoculum supplementation with 1% glucose (v/v) and addition of 0.1 mM $ZnSO_4$ to

the main culture. Protein expression was verified, as seen in **Fig. 1**, with expression induction being initiated at a lower OD_{600} (0.65) than Langelier et al., [16].

Difficulties in the expression of PARP1 may be related to the toxicity due to its enzymatic activity [6], but also to the complex structure and folding capability of the protein. It is likely that the addition of zinc into the growth media, allowed for a stabilization of the zinc-finger domain, and thus the overall stability of the protein structure [16]. It's important to emphasize that contrary to the Langelier et al., [16] expression protocol, our adapted procedure does not resort to the use of any type of PARP1 inhibitor (benzamide), thus leaving our recombinant protein close to its biologically active state. Furthermore, it is important to note that the ability of Rosetta 2 to express this protein may be linked to its utility in the expression of human recombinant proteins, having present a chloramphenicol-resistant plasmid that encodes tRNA genes for seven rare codons in *E.coli* (AGA, AGG, AUA, CUA, GGA, CCC and CGG) [18].

3.2. PARP1 Purification

After the determination of optimal expression conditions, a large-scale expression was performed in a 1 L culture, followed by protein purification. The purification protocol involved the use of a 1 ml Histrap and a 5 ml Heparin column. From the Histrap column, PARP1 was eluted at ~20% buffer B, and the use of a 5% buffer B step before the gradient removed a large part of contaminating *E. coli* proteins, as shown in the chromatogram profile of **Fig. 2a and b**. From the analysis of the 254 nm chromatogram profile, PARP1 appears to be bound to DNA (**Fig. 2a**). Because of this and the knowledge that the Zinc fingers (Zn1-3) [6,19] and WGR domain are capable of binding nucleic acids [20], we decided to proceed with a Heparin purification step.

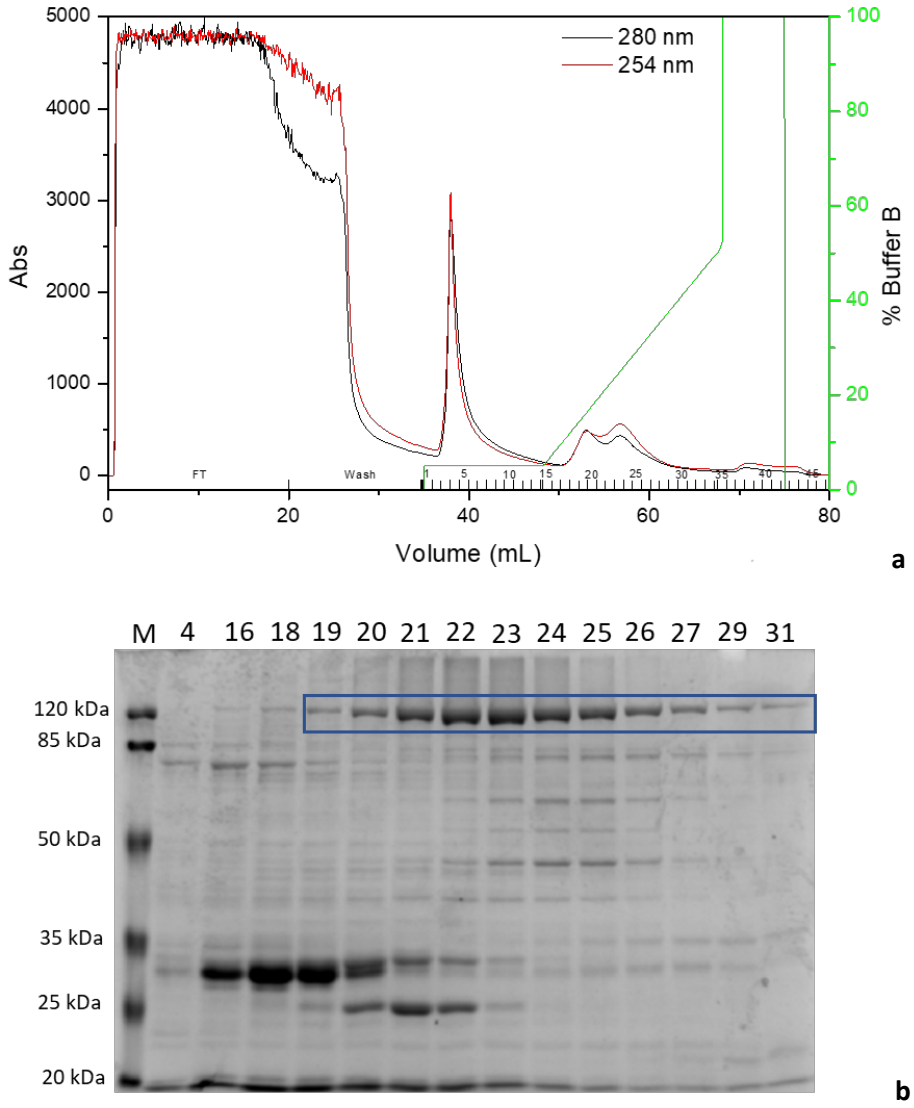

Figure 2. Histrap purification of PARP1. **a**) Chromatogram of HisTrap purification. A large amount of contaminating proteins from *E. coli* were removed with a 5% buffer B step and the protein of interest was eluted in approximately 20% buffer B. **b**) SDS-PAGE analysis of Histrap purification. Fractions that were analysed are identified with their respective fraction number and fractions pooled are selected in a blue frame. M - Precision Plus Protein™ Dual color standard (BioRad)).

Prior to the Heparin purification, a sample desalting (HiPrep™ 26/10 Desalting) was conducted to remove imidazole and reduce the salt concentration. Desalted fractions were injected into the 5 ml Heparin column, and a gradient from 0 to 100 % buffer B (50 mM Tris-HCl pH 8.0, 1 M NaCl, 0.1 mM TCEP, 1 mM EDTA) was employed to purify PARP1. In **Fig. 3** it can be observed that we were able to remove several contaminants, and that PARP1 presents low to medium affinity to the Heparin resin, with the elution occurring at approximately 45-50 % buffer B (**Fig. 3a**). It should be noticed that the low to medium affinity to the column may be an indication of the

native affinity of PARP1's WGR and Zn domains to nucleic acids. Also, a variation in binding affinity to the column may be explained by differences in protein folding. The WGR domain is a domain that is conserved among the three nuclear human PARPs (1-3), where it has a central role in DNA dependent regulation of PARP 2 and 3 repair activity [21]. While PARP1's DNA dependent activity solely rely on the Zn1 and 3 domains, PARP2 recruitment to DNA breaks is orchestrated by the WGR and CAT domain [22].

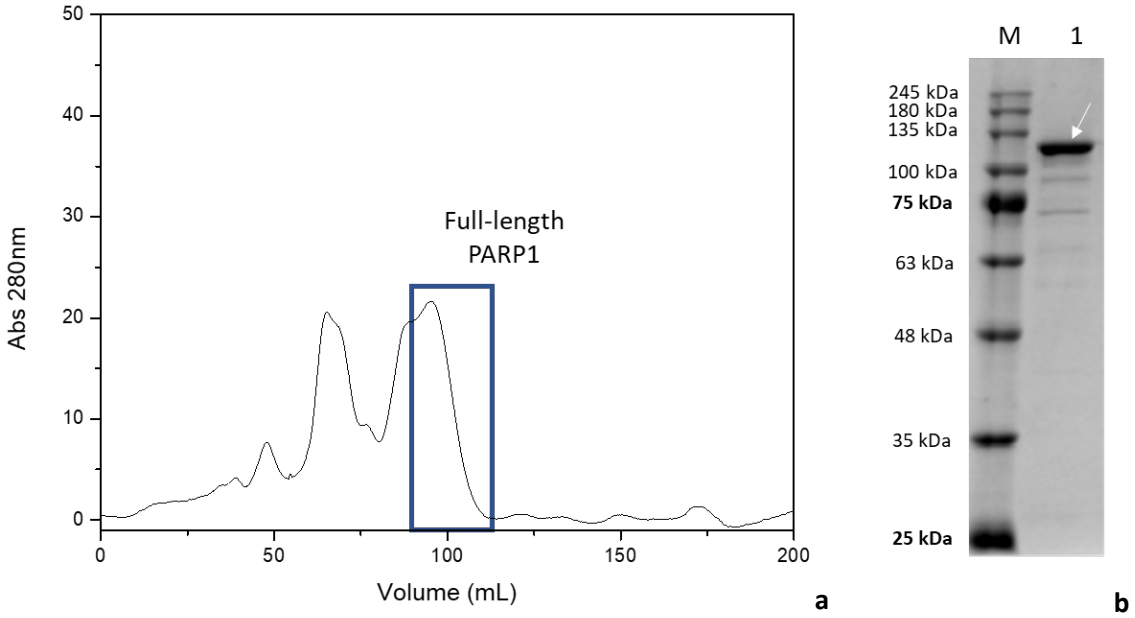

Figure 3. Heparin purification of PARP1 for DNA removal. a) Chromatogram for Heparin purification. A gradient of 0-100 % buffer B was used, and the protein was eluted at 45-50 % buffer B. The fractions selected and pooled for analysis on SDSPAGE gel are identified in the dark blue frame, b) SDS-PAGE gel analysis of Heparin purification, M – NZYColour Protein Marker II (NZYTech); 1- Pooled fractions of PARP1.

Upon finalization of the Heparin purification, selected protein fractions were analysed in a polyacrylamide gel, results shown in **Fig. 3b**. This assessment revealed that PARP1 presented a high degree of purity (> 95 %). Protein yield after Heparin purification was 3.5 ± 0.3 mg.

3.3. Protein Purity Evaluation and Yield

In order to further analyse the purity of PARP1, aliquots of Heparin purified samples were analysed by gel filtration using a Superdex 200 10/300GL column (24ml column). In **Fig. 4a** and **b** it can be observed that PARP1 is eluted from the column at 12 ml volume and appears in the chromatogram as a single isolated peak. Thus, we can state that a two-step purification is sufficient for PARP1 purification.

Even though pure PARP1 is achieved after heparin purification and can be used in biophysical and biochemical characterization studies, we would like to emphasize that in the case of protein structural analysis (e.g. crystallography or cryo-EM) it is advised to proceed with a SEC step to ensure that any type of aggregates or trace elements from purification/storage buffer are removed.

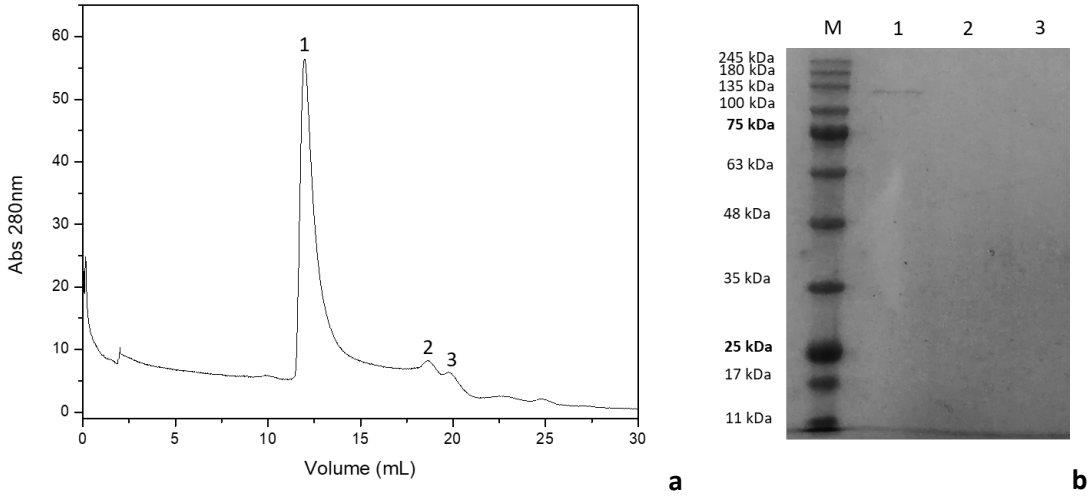

Figure 4. Size exclusion chromatography analysis of PARP1. a) Superdex 200 10/300GL (24 ml column) analysis of PARP1 with the presence of protein peak of interest at 12 ml elution volume. Peak 2 and 3 appear to be some small trace elements besides protein, that we hypothesise to be some RNA traces. b) PARP1 peak fractions analysed by SDS-PAGE: M - NZYColour Protein Marker II (NZYTech); 1 – fraction eluted at 12 ml; 2 – fraction eluted at 18.6 and 3- fraction eluted at 19.8 ml.

The use of a two-step purification procedure for PARP1 opens new possibilities in decreasing protein loss, which usually is associated with a multi-step purification process, as well as reducing protein stability problems due to exposure to environmental temperature variations.

An evaluation of the protein yield along the expression and purification process (**Table 3**) show great differences in values. We verified that after expression, the cell mass was approximately 4 g/l and that after the first purification step (Histrap) the protein mass was of 4.1 ± 0.3 mg. The protein yield significantly changed in the final purification step, with PARP1 presenting a total mass of 3.5 ± 0.3 mg. However, the concentration procedure showed to have a great impact on the complete process, as can be observed from **Table 3**. The final yield, after protein concentration was only 0.24 ± 0.02 mg, and translates into a reduction of protein mass of around 90 %, while it before concentration is only 14.6 %.

It´s important to emphasise that the major loss is due to the concentration process. We have indications that this was caused by the proteins interaction with the membrane from the Amicon

system. Upon experimenting with different centrifugation systems (Amicon, DiaFlow and Vivapore) and different membrane materials (cellulose and PES), we verified that the protein loss was similar or even greater (results not shown) than the values here depicted, using the Amicon® Ultra-4 (10 kDa MWCO) system.

To our knowledge, the problems with a massive loss of PARP1 during the concentration step has not been reported previously in the literature. However here we observed this phenomenon and suggest that care should be taken at this critical step, while attempting to obtain pure recombinant PARP1 protein. The resort to non-ionic detergents, such as NP40, is a common alternative in purification procedures and can be taken into consideration if a further increase in protein yield values is needed. Detergents are used to reduce protein-protein association and protein loss due to adsorption to surfaces [23]. However, because of detergents interference with or loss of sensitivity to protein characterization techniques (e.g. MS), protein quantification methods (e.g. Bradford method) and biochemical assays (e.g. protein-protein/lipid interaction assays), we did not include it in our purification protocol [23,24].

Table 3

PARP1 large-scale expression and purification yields.

Protein Expression (1L)	Cell Mass (g)	Histrap Protein Yield (mg)	Heparin Protein Yield (mg)	Final Yield (mg)
PARP1	4.8 ± 0.3	4.1 ± 0.3	3.5 ± 0.3	0.24 ± 0.02

*mean ± SD values

Although we identified the concentration step as one of the major critical points in PARP1's purification process, the quantification procedure also proved to be complicated. Quantification using the Nanodrop (absorbance at 280 nm – A_{280nm}) proved to be inefficient. We consider this problem to be related to PARP1's intrinsic low aromatic residue composition (1.3 % tryptophan, 3.2 % tyrosine and 3.0 % phenylalanine), but also to the protein folding. Depending on the three-dimensional structure of a protein in solution, residues can be more or less exposed to the surrounding environment, and this will affect the UV light absorption of the aromatic rings in the 280, 275 and 258 nm wavelengths [25]. Due to this problem, we resorted to the Bradford method. This method revealed to be a reliable alternative. Nevertheless, several limitations are associated with this quantification procedure, such as dye interaction or incompatibility to some

buffers/additives and problems related to proper protein standard selection [24]. In the present case, we selected bovine serum albumin (BSA) as our standard for protein quantification curves.

In summary, a fast and easy PARP1 purification protocol was developed, requiring a minimum number of steps to obtain pure protein. The PARP1 protocol required a 2-step purification, and the protein mass loss was reduced to a minimum. In the literature most laboratories refer to the Langelier's 3-step protocol (Histrap, Heparin and SEC) [5,11–14]. A direct comparison of our yield to the Langelier protocol is difficult since the latter does not give any exact number which we can compare with [11]. However, they claim that the yield is sufficient for structural and biophysical studies, which is also true for the outcome of our purification, it should thus be similar. However, in our case we report the yield from expression in one litre culture, while Langlier et al. has used 6 litres. Regarding the purity, a comparison of our protein in the SDS-PAGE gel in Figure 3b in this work and Figure 1 in Langlier et al., 2011 [11] demonstrate that there are some contaminants in the same size range for both samples. The purity is thus similar for the two samples.

Thus, following our 2 step protocol, the yield and the purity of PARP1 is comparable to previously published protocols, however the SEC purification and an additional protein concentration step can be dismissed, which thus simplifies he purification procedure, and in our case reduced the loss of protein during an additional purification and protein concentration step. Additionally, we are using a Tris-HCl buffer pH 8.0 for all the purification steps, which has not been reported before. This removes the need for an eventual buffer exchange and contributes to a further simplification of the protocol.

3.4. Western blot and PARP1 MS analysis for target confirmation

A qualitative analysis was performed by SDS-PAGE (**Fig. 5a**) and WB (to confirm protein target) (**Fig. 5b**), followed by MS analysis. In **Fig. 5a,** it is observed that PARP1 was purified, with a low amount of contaminant proteins, and that a relatively high purity value (> 95 %) was attained. However, trace amounts of contaminants between 75 to 100 kDa region are still observed (**Fig. 5a**).

Western blot assessments, by detection of the 6x Histag tail motifs, unequivocally identified the protein by band detection in the expected molecular mass region of PARP1 (114 kDa) (**Fig. 5b**). It is also important to emphasize that no contaminant was detected by this technique, which is a good indication of the integrity state of the protein of interest.

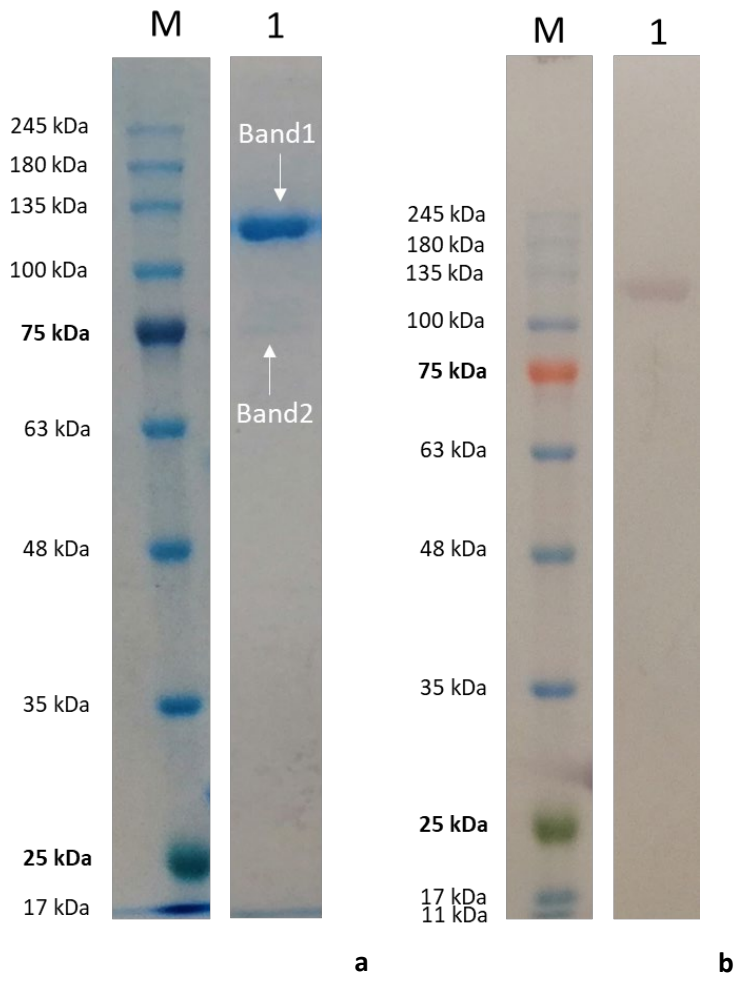

Figure 5. Purified recombinant human PARP1 protein analysis by SDS-PAGE gel (a) and western blot (b). M- NZYColour Protein Marker II (NZYTech); 1 – PARP1 (identification of Band1 and 2 analysed by Mass-spectrometry).

To ensure the identity of the expressed and purified PARP1 protein, the 114 kDa band (identified as Band1) and the 75 kDa contaminant band (identified as Band2) (**Fig. 5a**) were analysed by mass spectrometry (MS). Results retrieved from nanoLC-MS (**Supplementary Fig. 5 and Supplementary Table 1**) presented unequivocal identification of Band1 as human PARP1 (**Supplementary Table 1**) and Band2 as the *E.coli* protein maltodextrin phosphorylase (P00490 – PHSM_ECOLI) (**Supplementary Table 2**), an enzymatic protein involved in *E.coli* carbohydrate metabolism[26,27]. For both identifications high degree of confidence was considered (> 95 %).

3.5. Protein qualitative confirmation/evaluation (Zincon and activity assays)

AdditionalPARP1 quality assessments were performed to ensure proper enzymatic activity and were focused on: 1) the determination of protein's zinc content and 2) PARP1's auto-modification activity. These assays make sense since PARP1's DNA dependent enzymatic activity solely relies on the zinc fingers (Z1-3), BRCT (BRCA-1 C-terminus fold) and CAT (catalytic)

domains. From the three, the Zn1-3 domain intervenes in the binding to DNA break loci, the CAT domain catalyses NAD+ molecules to build poly(ADP- ribose) (PARP) chains (on itself or other protein targets) and the BRCT is pointed as the auto-modification domain, where PAR chains addition leads to PARP1 release from the break site [2,5,6,28].

Zinc fingers (ZF) are one of the most abundant motifs in proteins and are involved in the coordination of zinc atoms by specific amino acid residues (cysteins (C) and histidines (H), but also in specific cases by aspartate (D) and glutamate (E)) [29]. One of the more conserved orientations in eukaryotes is the CCHH, a classical ββα-fold, but other non-classical forms have also been identified, where C and H combinations differ [29,30]. These motifs are of key importance in molecular functions that require protein-DNA/RNA, protein-protein and protein-PAR interactions[30]. PARP1's three ZF domains are oriented by two CCHC and one CCCC in the Zn1, Zn2 and Zn3, respectively. Zn1-2 participate in DNA binding and Zn3 is responsible for interdomain interactions [31,32].

The Zn^{2+} quantification was performed using the chelating agent Zincon (2-carboxy-2'-hydroxy-5'-sulfoformazylbenzene) and a zinc ion standard curve was prepared (**Supplementary Fig. 6**). Results revealed that the purified protein presented a 1.1 ± 0.2 μM concentration of Zn^{2+}, which translates in a 1:1 protein:ion ratio. This value was inferior to what was expected of a three ZF domain protein (1:3) and could be justified by: 1) the technique's indirect detection mode, 2) the dependency on the effectiveness of the Zincon chelator reagent, and 3) an inefficient protein denaturation with urea. This last problem could be solved by increasing denaturant concentration and/or addition of guanidine hydrochloride (GdnHCl) [17], that will help to increase the availability of metalloprotein ions to chelation agents [17,33]. In addition, Bossak and colleagues [31] have previously presented evidence that point to an incomplete allocation of Zn^{2+} to PARP1 ZFs, which may explain part of the discrepancy between expected and observed zinc concentration. The authors verified that Zn^{2+} dissociation constants for Zn1 and Zn2 significantly differed, with values of 26 ± 4 nM and 4 ± 1 pM respectively. Zn1 low affinity to Zn^{2+} was suggested as an indication of Zn1 domain in a "metal-free" state, in the biological environment [31]. The incomplete Zn^{2+} allocation could partially explain the 1:1 protein/metal ion ratio detected by us, but also incomplete metal ion removal from PARP1's metal coordination core and subsequent reduced chelator interaction can justify the results obtained.

Additionally, we cannot rule out the chelator effect of the EDTA present in the purification buffer that could have some impact in the metal ion content of the protein. However, by the Zincon assay we were able to verify that the EDTA chelation effect wasn't complete, since zinc ions were detected. This event could be due to the protein folding state and/or to protein-protein

interactions, that could prevent complete metal ion depletion or slow-down metal ion dissociation, stabilizing the metal cores. This was previously reported with Ca^{2+}-binding proteins [34].

An auto-modification activity assay, following Langelier's protocol [16], was employed to confirm PARP1's DNA binding capability and DNA dependent enzymatic activity. PARP1 is incubated in a 1:1 ratio with a DNA template and upon addition of the NAD+ cofactor the formation of PAR chains (PARylation) onto itself is triggered. The post-translational modification serves as a mean for PARP1's release from DNA molecule and recruitment of repair effectors [28]. PARylation contributes to PARP1's size/weight increase, which can be visualized in an SDS-PAGE gel by a shift in the protein band to higher weight values. In **Fig. 6**, a shift is observed on PARP1's band localization to a higher molecular mass region, when compared to the negative control (CN). It is verified that the protein activity is triggered within seconds, and that the intensity of the unmodified protein band (114 kDa) decreases with time, while the intensity of the modified protein band is sharpened. A smear pattern is observed in the concentration gel portion at the 10-minute reaction time point, which serves as indication that further protein size increase occurs.

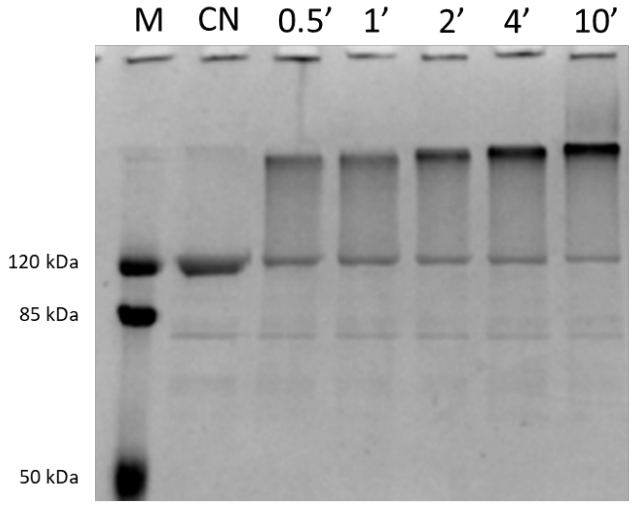

Figure 6. PARP1 auto-modification activity assay with analysis of different reaction time points. M-Protein marker III (VWR); CN – negative control; X' – reaction time (minutes).

PARP1's qualitative analysis revealed that the purified protein is fully active and that interaction with DNA occurs even at a low Zn^{2+}: protein ratio. Differences between expected and observed Zn^{2+}: protein ratio may be related to incomplete metal ion allocation, incomplete metal ion removal from PARP1's metal coordination core in the Zincon assay and partial EDTA chelation

effect. However, the detected Zn^{2+} content proved to be sufficient for DNA binding and subsequently to trigger PARP1's DNA dependent auto-modification activity.

3.6. Buffer thermostability assessment

Thermostability analysis was performed by means of intrinsic fluorescence emission spectrometry (Nano-DSF). Four different buffers (Tris-HCl, HEPES, Tricine and Gly-Gly) at three different pH (7.0, 7.5 and 8.0) conditions were assessed (**Supplementary Fig. 7**). Results indicated that stabilization was attained in all buffers, by the observation of a single peak denaturation profile (**Fig. 7** and **Supplementary Fig. 7 a-c**). The highest melting temperature (Tm) was verified at pH 8.0, with values ranging from 43 to 44 degrees (**Table 4**). An overall increase in Tm is verified with the increase in the ionic strength of the buffer. Tris-HCl (50 mM) at pH 8.0 presented the highest Tm value (44.2 ± 0.3 ^{o}C), when compared to remaining buffers. Tm differences between Tris-HCl and other buffers, at pH 8.0, present statistical significance ($p < 0.05$), except with Tricine (**Supplementary Table 3**). Tm variation in Tricine vs. Gly-Gly and HEPES vs. Tricine/Gly-Gly at pH 8.0, did not present statistical significance ($p \geq 0.05$). In terms of biological significance (≥ 3 ^{o}C) this is only verified in Tris-HCl buffer when pH 7.0 and pH 7.5/8.0 are compared, which in turn also presents statistical significance ($p < 0.05$).

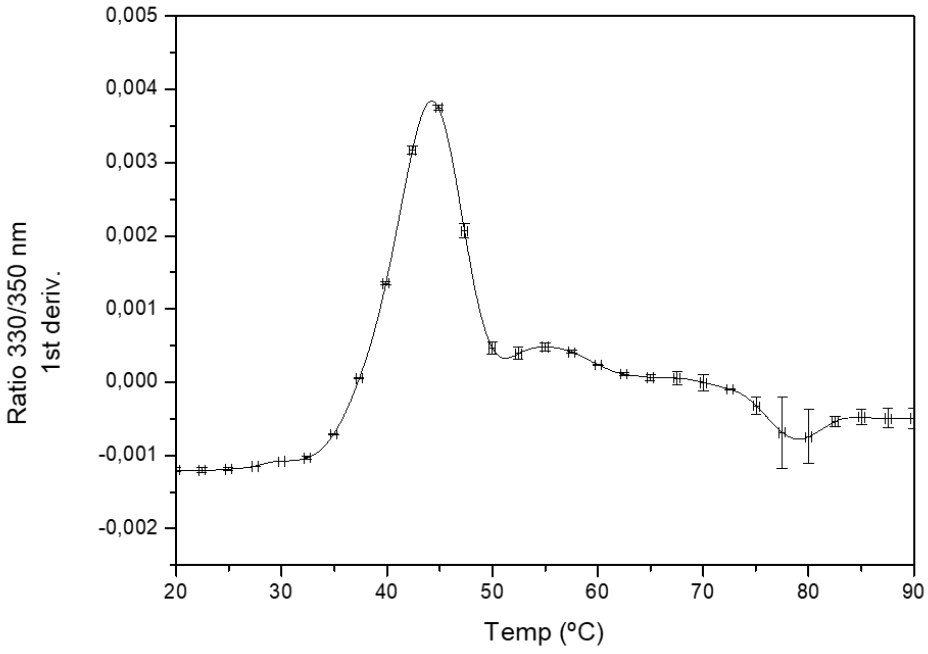

Figure 7. PARP1 buffer stabilization assessment by Nano-DSF. PARP1 stabilization curve (1st derivative 330/350 nm ratio) with buffer 50 mM Tris-HCl pH 8.0.

Table 4

PARP1 determined melting temperatures for assessed buffers and pH values.

	PARP1*			
	50 mM Tris-HCl	20 mM HEPES	50 mM Tricine	50 mM Gly-Gly
pH 7.0	39.3 ± 0.2	39.3 ± 0.1	N/A	39.8 ± 0.1
pH 7.5	43.0 ± 0.3	41.9 ± 0.1	N/A	42.0 ± 0.2
pH 8.0	44.2 ± 0.3	43.7 ± 0.2	44.2 ± 0.5	43.3 ± 0.4

*mean ±SD value

In sum, protein stabilization was achieved for PARP1, however additional work can also be carried out in further improving protein thermostability. This may be devised and supported by the buffer and pH conditions that rendered the best results (50 mM Tris-HCl pH 8.0) in this work. Salt and additives are good options for these further assessments. Specific stabilization conditions can be expected, and "tailor-made" buffers are required for optimal stabilization.

4. Conclusions

A user-friendly optimized protocol for expression, and purification of PARP1 was developed and analysed. Purification with high purity yields was achieved by means of a two-step protocol. However, elevated levels of protein loss were observed along the complete process, with the concentration procedure being the major limiting factor.

The purification protocol was optimized with as few steps as possible, making the complete purification process simpler. With this protocol there is only a need for two main purification steps (Histrap and Heparin) (**Fig. 8**). The SEC purification, that is associated with great protein loss, was abolished. Moreover, our protocol was optimized to reduce the number of protein concentration cycles (**Fig. 8**), thus decreasing the protein loss. The present work demonstrates that it is possible to purify PARP1 to an apparent purity of > 95% following a 2-step protocol. The SEC purification can be dismissed, and concentration cycles decreased to a minimum. Thus, making the reported protocol a fast and easy stepwise procedure to obtain pure and biologically

active protein. The protein sample obtained is close to its biological active human state and is thus suitable for biochemical and biophysical characterization studies. However, in case of structural studies (e.g. crystallography and cryo-EM) we advise that a SEC purification should be done to ensure removal of possible aggregates and/or buffer trace elements, but it should be kept in mind that the protein yield will be lower.

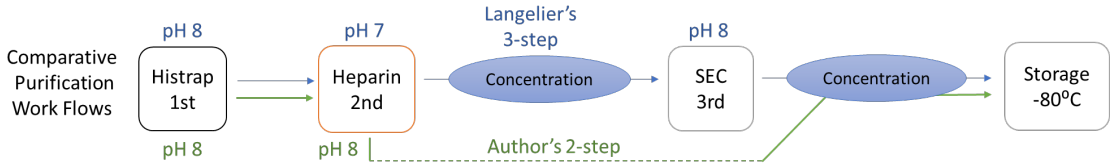

Figure 8. Purification workflow. A schematic comparison of the 3-step (Langelier et al. [16]) and 2-step (Author's present work) PARP1 purification protocols.

Additionally, a positive identification and confirmation of PARP1 purification was conducted by MS and WB.

A qualitative analysis performed on PARP1 samples demonstrated its DNA-binding aptitude and enzymatic capability. Even though the Zn^{2+} content revealed a possible incomplete metal bound state for the zinc finger domains, previously reported evidence corroborates a possible Zn1 domain "metal free-state".

Thermostability assessments by Nano-DSF allowed to determine the best buffer and pH conditions for protein purification and storage. PARP1 stabilization was achieved with 50 mM Tris-HCl pH 8.0, with an observation of a single unfolding peak and determination of Tm = 44.2 ± 0.3 ^{o}C.

Author contributions

Elin Moe: Conceptualization, Supervision, Project management, Methodology, Writing - Reviewing and Editing. Carlota J.F. Conceição: Investigation, Methodology, Visualization, Funding acquisition, Writing - Original draft preparation, reviewing and editing. Bruno Salgueiro: Methodology, Writing - Reviewing and Editing. Paulo A. Ribeiro: Supervision, Project management, Funding acquisition, Writing - Reviewing and Editing. Maria Raposo: Conceptualization, Supervision, Project management, funding acquisition, Writing - Reviewing and Editing.

Funding Statement

This research was funded by the Portuguese National Funding Agency (FCT-MCTES), Radiation Biology and Biophysics Doctoral Training Programme (RaBBiT, PD/00193/2012), the Applied Molecular Biosciences Unit—UCIBIO (UIDB/04378/2020), the CEFITEC Unit (UIDB/00068/2020), UIDB/04559/2020 (LIBPhys) and UIDP/04559/2020 (LIBPhys), the scholarships grant number PD/BD/142765/2018 and COVID/BD/152660/2022, to C.J.F.C. from the RaBBiT Doctoral Training Programme, and the project LISBOA-01-0145-FEDER-007660 (Microbiologia Molecular, Estrutural e Celular) funded by FEDER funds through COMPETE2020. B.S. acknowledge the funding from (DOCTOrates 4 covid-19 2020.08066.BD) PhD Programme in Molecular Biosciences.

Conflict of interest

The Authors declare no conflict of interest.

Acknowledgements

The Authors acknowledge Sandra Santos, Filipe Rollo, Andreia Fernandes and Catarina Paiva for technical assistance. The Merck Unit at ITQB/iBET for NanoDSF and Tecan equipment availability and usage. The Mass Spectrometry Unit (UniMS), ITQB/iBET, Oeiras, Portugal for providing the MS data.

Appendix A. Supplementary data

Supplementary data to this article can be found at: https://ars.els-cdn.com/content/image/1-s2.0-S1046592823001079-mmc1.docx

References

[1] S. Vyas, M. Chesarone-Cataldo, T. Todorova, Y. Huang, P. Chang, A systematic analysis of the PARP protein family identifies new functions critical for cell physiology, Nat. Commun. 4 (2013) 1–13. https://doi.org/10.1038/ncomms3240.

[2] L. van Beek, É. McClay, S. Patel, M. Schimpl, L. Spagnolo, T. Maia de Oliveira, Parp power: A structural perspective on parp1, parp2, and parp3 in dna damage repair and nucleosome remodelling, Int. J. Mol. Sci. 22 (2021) 1–23. https://doi.org/10.3390/ijms22105112.

[3] S.J. Baptista, M.M.C. Silva, E. Moroni, M. Meli, G. Colombo, T.C.P. Dinis, J.A.R. Salvador, Novel PARP-1 Inhibitor scaffolds disclosed by a dynamic structure-based

pharmacophore approach, PLoS One. 12 (2017) 1–20. https://doi.org/10.1371/journal.pone.0170846.

[4] F.G. Sousa, R. Matuo, D.G. Soares, A.E. Escargueil, J.A.P. Henriques, A.K. Larsen, J. Saffi, PARPs and the DNA damage response, Carcinogenesis. 33 (2012) 1433–1440. https://doi.org/10.1093/carcin/bgs132.

[5] J.D. Steffen, R.M. Tholey, M. Langelier, J.L. Planck, J. Schiewer, S. Lal, N.A. Bildzukewicz, C.J. Yeo, K.E. Knudsen, J.R. Brody, J.M. Pascal, Targeting PARP-1 allosteric regulation offers therapeutic potential against cancer, Cancer Res. 74 (2015) 31–37. https://doi.org/10.1158/0008-5472.CAN-13-1701.

[6] J.M. Dawicki-McKenna, M.F. Langelier, J.E. DeNizio, A.A. Riccio, C.D. Cao, K.R. Karch, M. McCauley, J.D. Steffen, B.E. Black, J.M. Pascal, PARP-1 Activation Requires Local Unfolding of an Autoinhibitory Domain, Mol. Cell. 60 (2015) 755–768. https://doi.org/10.1016/j.molcel.2015.10.013.

[7] E.E. Alemasova, O.I. Lavrik, Poly(ADP-ribosyl)ation by PARP1: Reaction mechanism and regulatory proteins, Nucleic Acids Res. 47 (2019) 3811–3827. https://doi.org/10.1093/nar/gkz120.

[8] Ke, Wang, Zhang, Zhong, Wang, Zeng, Ba, The Role of PARPs in Inflammation—and Metabolic—Related Diseases: Molecular Mechanisms and Beyond, Cells. 8 (2019) 1047. https://doi.org/10.3390/cells8091047.

[9] N. V. Maluchenko, A. V. Feofanov, V.M. Studitsky, PARP-1-Associated Pathological Processes: Inhibition by Natural Polyphenols, Int. J. Mol. Sci. 22 (2021) 11441. https://doi.org/10.3390/ijms222111441.

[10] K. Mao, G. Zhang, The role of PARP1 in neurodegenerative diseases and aging, FEBS J. 289 (2022) 2013–2024. https://doi.org/10.1111/febs.15716.

[11] J.M. Langelier, MF; Planck, JL.; Servent, Kristin M.; Pascal, Purification of Human PARP-1 and PARP-1 Domains from Escherichia coli for Structural and Biochemical Analysis, in: A. V. Tulin (Ed.), Poly Polym. Methods Protoc., Humana Press, Totowa, NJ, 2011: pp. 93–115. https://doi.org/10.1007/978-1-61779-270-0.

[12] J. Rudolph, U.M. Muthurajan, M. Palacio, J. Mahadevan, G. Roberts, A.H. Erbse, P.N. Dyer, K. Luger, The BRCT domain of PARP1 binds intact DNA and mediates intrastrand transfer, Mol. Cell. 81 (2021) 4994-5006.e5. https://doi.org/10.1016/j.molcel.2021.11.014.

[13] M.F. Langelier, R. Billur, A. Sverzhinsky, B.E. Black, J.M. Pascal, HPF1 dynamically controls the PARP1/2 balance between initiating and elongating ADP-ribose modifications, Nat. Commun. 12 (2021). https://doi.org/10.1038/s41467-021-27043-8.

[14] N.J. Clark, M. Kramer, U.M. Muthurajan, K. Luger, Alternative modes of binding of poly(ADP-ribose) polymerase 1 to free DNA and nucleosomes, J. Biol. Chem. 287 (2012) 32430–32439. https://doi.org/10.1074/jbc.M112.397067.

[15] G. Liszczak, K.L. Diehl, G.P. Dann, T.W. Muir, Acetylation blocks DNA damage–induced chromatin ADP-ribosylation, Nat. Chem. Biol. 14 (2018) 837–840. https://doi.org/10.1038/s41589-018-0097-1.

[16] M.F. Langelier, J.D. Steffen, A.A. Riccio, M. McCauley, J.M. Pascal, Purification of DNA Damage-Dependent PARPs from E. coli for Structural and Biochemical Analysis, Methods Mol Biol. 1608 (2017) 431–444. https://doi.org/10.1007/978-1-4939-6993-7_27.

[17] C.E. Säbel, J.M. Neureuther, S. Siemann, A spectrophotometric method for the determination of zinc, copper, and cobalt ions in metalloproteins using Zincon, Anal. Biochem. 397 (2010) 218–226. https://doi.org/10.1016/j.ab.2009.10.037.

[18] J.L. Kopanic, M. Al-Mugotir, S. Zach, S. Das, R. Grosely, P.L. Sorgen, An Escherichia coli strain for expression of the connexin45 carboxyl terminus attached to the 4th transmembrane domain, Front. Pharmacol. 4 (2013). https://doi.org/10.3389/fphar.2013.00106.

[19] J.D. Steffen, M.M. McCauley, J.M. Pascal, Fluorescent sensors of PARP-1 structural dynamics and allosteric regulation in response to DNA damage, Nucleic Acids Res. 44 (2016) 9771–9783. https://doi.org/10.1093/nar/gkw710.

[20] M.F. Langelier, J.L. Planck, S. Roy, J.M. Pascal, Structural Basis for DNA Damage–Dependent Poly(ADP-ribosyl)ation by Human PARP-1, Science (80-.). 336 (2012) 728–732. https://doi.org/10.1126/science.1216338.

[21] M.F. Langelier, A.A. Riccio, J.M. Pascal, PARP-2 and PARP-3 are selectively activated by 5’ phosphorylated DNA breaks through an allosteric regulatory mechanism shared with PARP-1, Nucleic Acids Res. 42 (2014) 7762–7775. https://doi.org/10.1093/nar/gku474.

[22] A.A. Riccio, G. Cingolani, J.M. Pascal, PARP-2 domain requirements for DNA damage-dependent activation and localization to sites of DNA damage, Nucleic Acids Res. 44 (2015) 1691–1702. https://doi.org/10.1093/nar/gkv1376.

[23] Y.-G. Yeung, E. Nieves, R.H. Angeletti, E.R. Stanley, Removal of detergents from protein digests for mass spectrometry analysis, Anal. Biochem. 382 (2008) 135–137. https://doi.org/10.1016/j.ab.2008.07.034.

[24] M.I. Knight, P.J. Chambers, Problems associated with determining protein concentration: A comparison of techniques for protein estimations, Appl. Biochem. Biotechnol. - Part B Mol. Biotechnol. 23 (2003) 19–28. https://doi.org/10.1385/MB:23:1:19.

[25] A.B. Biter, J. Pollet, W.-H. Chen, U. Strych, P.J. Hotez, M.E. Bottazzi, A method to probe protein structure from UV absorbance spectra, Anal. Biochem. 587 (2019) 113450. https://doi.org/10.1016/j.ab.2019.113450.

[26] R. Dippel, W. Boos, The maltodextrin system of Escherichia coli: metabolism and transport., J. Bacteriol. 187 (2005) 8322–31. https://doi.org/10.1128/JB.187.24.8322-8331.2005.

[27] H. Nakai, M.J. Baumann, B.O. Petersen, Y. Westphal, H. Schols, A. Dilokpimol, M.A. Hachem, S.J. Lahtinen, J.Ø. Duus, B. Svensson, The maltodextrin transport system and metabolism in Lactobacillus acidophilus NCFM and production of novel α-glucosides through reverse phosphorolysis by maltose phosphorylase, FEBS J. 276 (2009) 7353–7365. https://doi.org/10.1111/j.1742-4658.2009.07445.x.

[28] P.A. Loeffler, M.J. Cuneo, G.A. Mueller, E.F. Derose, S.A. Gabel, R.E. London, Structural studies of the PARP-1 BRCT domain, BMC Struct. Biol. 11 (2011) 37. https://doi.org/10.1186/1472-6807-11-37.

[29] K. Kluska, J. Adamczyk, A. Krężel, Metal binding properties of zinc fingers with a naturally altered metal binding site, Metallomics. 10 (2018) 248–263. https://doi.org/10.1039/c7mt00256d.

[30] M. Cassandri, A. Smirnov, F. Novelli, C. Pitolli, M. Agostini, M. Malewicz, G. Melino, G. Raschellà, Zinc-finger proteins in health and disease, Cell Death Discov. 3 (2017). https://doi.org/10.1038/cddiscovery.2017.71.

[31] K. Bossak, W. Goch, K. Piatek, T. Fraczyk, J. Poznański, A. Bonna, C. Keil, A. Hartwig, W. Bal, Unusual Zn(II) Affinities of Zinc Fingers of Poly(ADP-ribose) Polymerase 1 (PARP-1) Nuclear Protein, Chem. Res. Toxicol. 28 (2016) 191–201. https://doi.org/10.1021/tx500320f.

[32] M.N. Wenzel, S.M. Meier-Menches, T.L. Williams, E. Rämisch, G. Barone, A. Casini,

Selective targeting of PARP-1 zinc finger recognition domains with Au(III) organometallics, Chem. Commun. 54 (2018) 611–614. https://doi.org/10.1039/c7cc08406d.

[33] S. Siemann, D. Brewer, A.J. Clarke, G.I. Dmitrienko, G. Lajoie, T. Viswanatha, IMP-1 metallo-β-lactamase: effect of chelators and assessment of metal requirement by electrospray mass spectrometry, Biochim. Biophys. Acta - Gen. Subj. 1571 (2002) 190–200. https://doi.org/10.1016/S0304-4165(02)00258-1.

[34] J.K. Nyborg, O.B. Peersen, That zincing feeling: the effects of EDTA on the behaviour of zinc-binding transcriptional regulators, Biochem. J. 381 (2004). https://doi.org/10.1042/BJ20041096.